GLIA

WILEY

RESEARCH ARTICLE

Inhibition of altered Orai1 channels in Müller cells protects photoreceptors in retinal degeneration

Basma Sukkar[1] | Lalehan Oktay[2] | Ayse Sahaboglu[3] | Aylin Moayedi[1] | Shima Zenouri[1] | Tamer Al-Maghout[4] | Antolin Cantó[5] | María Miranda[5] | Serdar Durdagi[2,6] | Zohreh Hosseinzadeh[1,7]

[1]Paul Flechsig Institute, Centre of Neuropathology and Brain Research, University of Leipzig, Leipzig, Germany

[2]Computational Biology and Molecular Simulations Laboratory, Department of Biophysics, School of Medicine, Bahcesehir University, Istanbul, Turkey

[3]Institute for Ophthalmic Research, Centre for Ophthalmology, Eberhard Karls University, Tübingen, Germany

[4]Department of Cardiology and Vascular Medicine and Physiology, University of Tübingen, Tübingen, Germany

[5]Departamento Ciencias Biomédicas, Facultad de Ciencias de la Salud, Universidad Cardenal Herrera-CEU, CEU Universities, Valencia, Spain

[6]Molecular Therapy Laboratory, School of Pharmacy, Bahcesehir University, Istanbul, Turkey

[7]Department of Ophthalmology and Eye Hospital, University of Leipzig, Leipzig, Germany

Correspondence
Zohreh Hosseinzadeh, Paul Flechsig Institute, Centre of Neuropathology and Brain Research, University of Leipzig, Leipzig, Germany.
Email: zohreh.hosseinzadeh@medizin.uni-leipzig.de

Abstract

The expressions of ion channels by Müller glial cells (MGCs) may change in response to various retinal pathophysiological conditions. There remains a gap in our understanding of MGCs' responses to photoreceptor degeneration towards finding therapies. The study explores how an inhibition of store-operated Ca^{2+} entry (SOCE) and its major component, Orai1 channel, in MGCs protects photoreceptors from degeneration. The study revealed increased Orai1 expression in the MGCs of retinal degeneration 10 (*rd10*) mice. Enhanced expression of oxidative stress markers was confirmed as a crucial pathological mechanism in *rd10* retina. Inducing oxidative stress in rat MGCs resulted in increasing SOCE and Ca^{2+} release-activated Ca^{2+} (CRAC) currents. SOCE inhibition by 2-Aminoethoxydiphenyl borate (2-APB) protected photoreceptors in degenerated retinas. Finally, molecular simulations proved the structural and dynamical features of 2-APB to the target structure Orai1. Our results provide new insights into the physiology of MGCs regarding retinal degeneration and shed a light on SOCE and Orai1 as new therapeutic targets.

KEYWORDS
MD simulations, molecular docking, Müller glial cells, Orai1, oxidative stress, retina, retinal degeneration, SOCE

1 | INTRODUCTION

MGCs, a predominant type of glial cells found in the vertebrate retina, are likely sensitive to changes in the status of photoreceptor cells in many ways. First, MGCs' processes protect retinal cells including the photoreceptors, and secondly, they support the photoreceptors (Reichenbach & Bringmann, 2020). MGCs contribute to pivotal cellular functions, including structural support, neurotransmitter recycling, glutamate metabolism, maintenance of the blood–retinal barrier (BRB), and energy provision (Eastlake et al., 2019). In addition, they regulate ion homeostasis through transmembrane ionic channels (Gao et al., 2021; Reichenbach & Bringmann, 2020). Moreover, MGCs upregulate the glial fibrillary acidic protein (GFAP), an intermediate filament protein considered a marker for reactive gliosis under retinal degeneration.

Calcium (Ca^{2+}) signaling is an important player in MGCs (Keirstead & Miller, 1995; Newman, 2015; Newman & Zahs, 1998). These ions are mainly obtained through either Ca^{2+} influx from the outer medium via several forms of Ca^{2+} channels, or Ca^{2+} reflux from intracellular Ca^{2+} stores, as endoplasmic reticulum (ER), followed by store-operated Ca^{2+} entry (SOCE) utilizing the pore-forming Ca^{2+} channel, Orai (Putney, 2007). In the retinal glial cells, Ca^{2+} released from ER is dependent on the activation of inositol trisphosphate (IP3) and/or ryanodine channels (Verkhratsky et al., 2013). The main astroglial SOCE conduit is the transient receptor potential cation (TRPC) channels. Synergistic activation of TRPC and Orai channels control SOCE in mouse MGCs (Molnár et al., 2016). Intraocular pressure is facilitated by a lack of TRPC1 (Molnár et al., 2016). In addition, SOCE is involved in Ca^{2+} homeostasis of rod photorecptors via TRPC1 channels (Verkhratsky et al., 2013). SOCE is induced by various stimuli including mechanical, osmotic, purinergic and cholinergic stimuli. Such stimulations elevate the cytosolic Ca^{2+} activity ($[Ca^{2+}]_i$) in astrocytes, leading to modulation of neuronal plasticity, downstream signaling, and local blood flow (Khakh & McCarthy, 2015; Newman, 2015; Ryskamp et al., 2015). Increased intracellular Ca^{2+} concentrations stimulate MGCs, resulting in subsequent ganglion cells hyperpolarization and the release of gliotransmitters such as glutamate, ATP, and adenosine (Reichenbach & Bringmann, 2013). Although we have gained knowledge about Ca^{2+} signaling in MGCs, SOCE-coupled Ca^{2+} Orai channels (SOCE/Orai) have been less studied.

The inhibition of SOCE channels of photoreceptors leads to diminished intracellular Ca^{2+} concentrations that results in blocking the synaptic release from horizontal and bipolar cells in both amphibian and mammalian retinas (Szikra et al., 2008; Szikra et al., 2009). Ca^{2+} signals have been studied further in retinal cells under retinal degeneration. Elevated intracellular Ca^{2+} concentrations are correlated to degeneration of photoreceptors in retinitis pigmentosa (RP) (Nakazawa, 2011).

In the developed world, RP is one of the leading global causes of blindness among the working age population (Herse, 2005; Tsang & Sharma, 2018). RP represents a group of inherited neurodegenerative diseases that cause selective cell death of photoreceptors followed by a decrease in the outer nuclear layer (ONL) thickness (Hood et al., 2011). Among the numerous mutations that lead to RP, the autosomal missense mutations of the phosphodiesterase 6 (PDE6) are the most common ones (Sakamoto et al., 2009; Wert et al., 2014). These mutations lead to an increased ion influx, particularly calcium, via opened cGMP-gated channels (Wang et al., 2018). This may influence calcium signals in retinal cell types, MGCs in particular. There is still a lack of knowledge concerning SOCE/Orai in MGCs in the case of RP. Therefore, this study investigates the regulation of Orai channels as the most important component of SOCE under the pathological status of RP. Here, our focus is Orai1, being one of the Orai isoforms in the retina (Sakamoto et al., 2009; Uhlén et al., 2015).

2 | RESULTS

2.1 | Orai1 expressions and activities of MGCs are increased in the rd10 retinas

In our observations, we found that Orai1, Orai2, and Orai3 were expressed in rat MGCs, as shown in Figure S1a-c. To investigate the potential modulation of Orai isoforms by oxidative stress in the context of retinal degeneration, we examined the expression levels of Orai1, Orai2, and Orai3 in MGCs treated with hydrogen peroxide (H_2O_2) for 2 h at a concentration of 1 μM. After treating rat MGCs with H_2O_2 (2 h, 1 μM), only Orai1 expression was significantly upregulated, as depicted in Figure S1a. Consequently, this study focused on the role of Orai1 in MGCs under stress and retinal degeneration. Next, Orai1 and GFAP expressions were analyzed via immunofluorescence detection on *ex vivo* retinal cryosections from wild type (*wt*) and *rd10* mice at P18, the peak of degeneration (Gargini et al., 2007; Vidal-Gil et al., 2019). Orai1 expression was observed in ONL, inner nuclear layer (INL) and ganglion cell layer (GCL) in both *wt* and *rd10* retinas (Figure 1a–f). For the evaluation of Orai1 expression, fluorescence intensity was analyzed by using ImageJ software. Immunopositivity for Orai1 showed a significant gradual increase of intensity for different layers (ONL-GCL) at P18 (Figure 1a,d). The intensity levels of Orai1 in *wt* and *rd10* retinas were significantly higher in GCL compared to INL and ONL (Figure 1a,d,g). Orai1 was significantly increased in *rd10* compared to *wt* in the layers (Figure 1g). In addition, GFAP was colocalized completely with Orai1 positivity at the inner plexiform layer (IPL) and outer plexiform layer (OPL) in *rd10* retinas (Figure 1c,f), in connection to increased MGCs activity. Furthermore, Orai1 mRNA levels were examined in *rd10* mouse strains and their corresponding littermates. Orai1 expression was higher in *rd10* retinas, compared to healthy retinas (Figure 1h).

To investigate whether the activities of Orai by Ca^{2+} store depletion with inositol trisphosphate (IP_3) could be changed under retinal degeneration in *rd10* mice, patch clamp experiments were conducted. Freshly isolated MGCs from retinas of *rd10* and healthy mice were measured using the patch clamp technique to analyze Ca^{2+} release-activated Ca^{2+} current (I_{CRAC}), which reflects Orai activities. The conductance of the inward current (randomly patched different parts of

FIGURE 1 Orai1 expression and current in *wt* and *rd10* mouse retinas. Analysis of Orai1 expression showed immunoreactivity in the ganglion cell layer (GCL), inner nuclear layer (INL), and retinal pigment epithelium (RPE) in *wt* retinas (a); and in outer nuclear layer (ONL), inner nuclear layer (INL), and GCL in *rd10* retinas at P18 (d); as indicated by arrows. GFAP immunoreactivity colocalized with Orai1 in *wt* and *rd10* retinas (c, f); quantitative analysis of fluorescence intensity levels of Orai1 in *wt* (blue bar) and *rd10* (orange bar) retinas in GCL compared to INL and ONL (G); arithmetic means (±SEM, $n = 4$) of normalized expression of Orai1 levels in retina from *wt* mice (blue bar) or *rd10* mice (orange bar) using GAPDH mRNA as a reference (h); a schematic figure of patch clamping of Müller cells as well as mean current–voltage (I/V) relationships of currents normalized to the capacitance of MGCs of *wt* retina (blue, $n = 14$, 6 retinas) and *rd10* retina (orange, $n = 13$, 6 retinas) following the addition of 40 μM IP$_3$ (i); Mean peak current density ± SEM ($n = 13$–14) measured at -10, -20, -30, -40, and -50 mV after the precondition potential to $+50$ mV in Müller cells from *wt* ($n = 14$, 6 retinas) and *rd10* retinas ($n = 13$, 6 retinas) following the addition of 40 μM IP$_3$ (j–n). $*p \le .05$, $**p \le .01$ indicates statistically significant difference, Kolmogorov–Smirnov test for multiple comparisons; the unpaired Student's t-test for one-to-one comparisons.
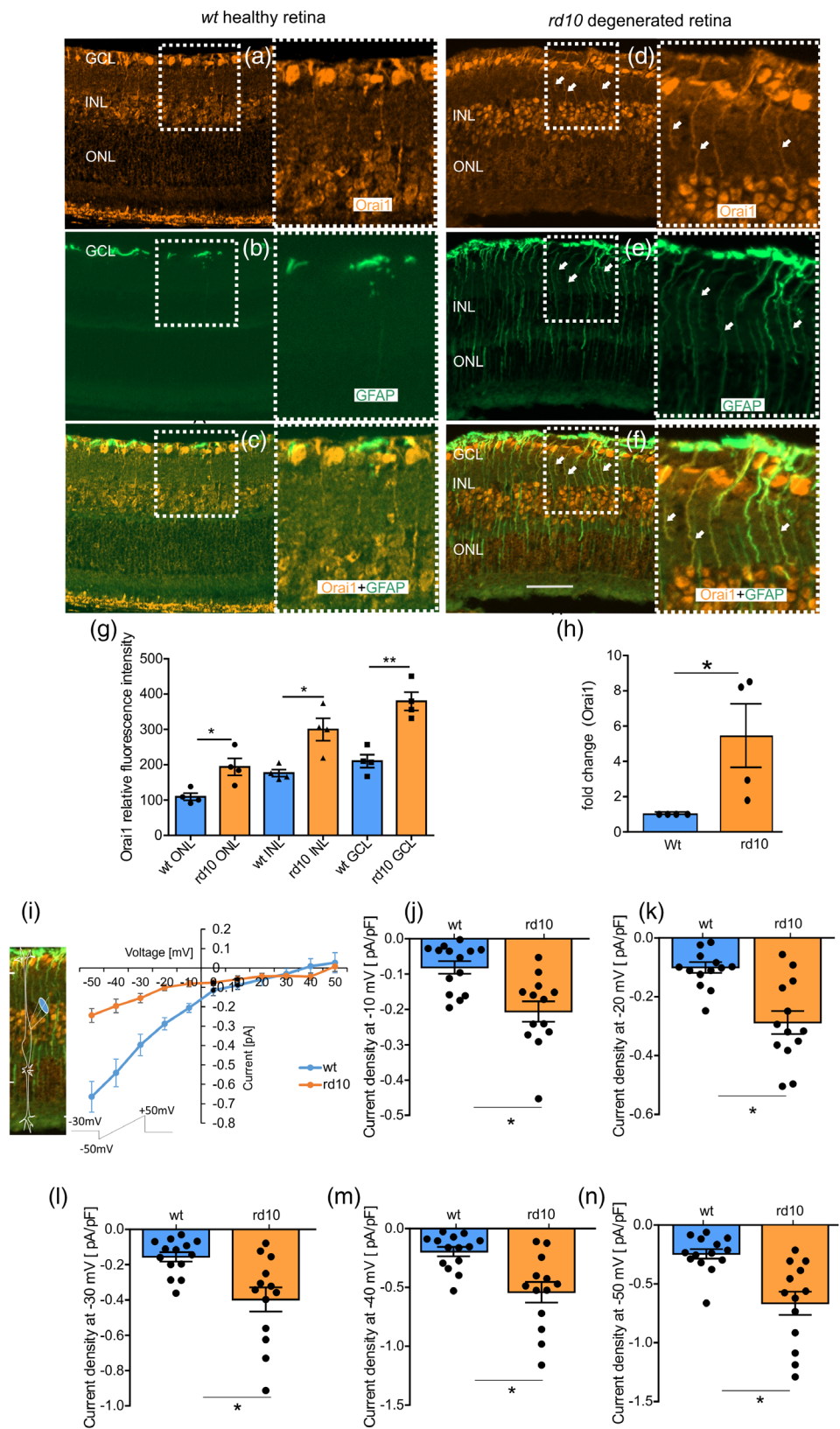
MGCs from proximal process to endfoot), triggered by Ca^{2+} store depletion with IP$_3$ in the pipette solution, was significantly increased in the MGCs of *rd10* mice (Figure 1j). Moreover, the current densities from -10 to -50 mV were higher in *rd10* retinas (Figure 1j-n).

2.2 | Oxidative stress is increased in rd10 retinas

To confirm that oxidative stress is an important pathological mechanism in the animal model used in this study, we have analyzed various

markers involved in oxidative stress, including the expression of hydroxynonenal (HNE), reduced and oxidized glutathione (GSH-GSSG), and the catalytic subunit of Glutamate cysteine ligase catalytic (GCLC) enzyme in retinal sections from *rd10* animals at P18.

Fluorescence intensity reflecting HNE expression, a product of lipid peroxidation, was quantified by using ImageJ software. HNE expression was observed in ONL, OPL, INL, IPL, and GCL (Figure 2a–e) in both *wt* and *rd10* retinas. The expression of HNE was significantly increased in the ONL of *rd10* retinas when compared to corresponding *wt* (Figure 2c). There were no significant differences in the expression of this oxidative stress marker in the OPL, INL, IPL, or GCL of *rd10* and *wt* retinas.

The expression of GSH-GSSG, the major intracellular antioxidant, was studied to understand the oxidative process in *rd10* and *wt* retinas. GSH-GSSG staining was found in ONL, OPL, INL, IPL, and GCL layers (Figure 2f–o). The percentage of the retinal area occupied by GSH-GSSG staining was quantified, and a significant increase in the ONL was found in the *rd10* retinas compared to *wt* retinas (Figure 2h).

GCLC, the rate-limiting enzyme in the de novo synthesis of GSH, was also studied. The expression of this enzyme was observed in the whole retina, and interestingly, it was significantly increased in the *rd10* retinas (Figure 2p–t). This increased GSH-GSSG expression may be a defense mechanism of the retina trying to synthesize new antioxidants when dealing with increased oxidative stress. HNE and GSH-GSSG expressions were not colocalized with GFAP expression (Figure 2d,e and Figure 2i,j), but this was observed in GCLC (Figure 2s,t), thus suggesting that GSH synthesis may occur in MGCs.

2.3 | SOCE activity of MGCs is increased under oxidative stress

To explore the effects of oxidative stress associated with retinal degeneration on Orai1 expression in MGCs, we exposed rat MGCs to H_2O_2 and evaluated SOCE activity. Rat MGCs were incubated with 1 μM H_2O_2 for 2 h. Afterward, the effect on SOCE was checked utilizing Fura2 fluorescence to quantify intracellular Ca^{2+} concentration $[Ca^{2+}]_i$.

To capture the activity of SOCE, MGCs were exposed to thapsigargin (1 μM), an inhibitor of the sarco−/ER Ca^{2+}-ATPase (SERCA). This was performed in the absence of extracellular Ca^{2+} to empty the intracellular stores (Bird et al., 2008) (Figure 3a). Re-addition of Ca^{2+} in the extracellular bath in the continued presence of thapsigargin resulted in an increase of $[Ca^{2+}]_i$, indicating increased SOCE function (Figure 3a). H_2O_2-treated MGCs showed a higher peak (Figure 3b,c) of SOCE compared to the control untreated group.

2.4 | CRAC current is increased in MGCs under H_2O_2-induced oxidative stress

The whole cell patch clamp recording was applied to analyze I_{CRAC} under oxidative stress in MGCs. As illustrated in Figure 3h,i, the

conductance of the inward current and current density, triggered by Ca^{2+} store depletion with IP$_3$ in the pipette solution, was significantly increased in MGCs treated with H_2O_2 (1 μM, 2 h).

To investigate the effect of oxidative stress on Orai1, western blot analysis was applied to test protein abundance (Figure 3j). The Orai1 protein abundance was significantly higher in H_2O_2-treated rat MGCs (Figure 3k). Similarly, enhanced mRNA of Orai1 was expected to be parallel with enhanced SOCE. Therefore, transcript levels encoding Orai1 were analyzed with qRT-PCR after H_2O_2 treatment, and the results revealed a significant increase in Orai1 transcript levels in H_2O_2-treated cells (Figure 3l). The results confirmed an incorporation between Orai1 and SOCE in stressed MGCs with H_2O_2 (Figure 3). Applying Orai1 inhibitors, including 2-APB (10 μM, 24 h), MRS-1845 (10 μM, 24 h), or GSK-7975A (1 μM, 24 h) eliminated this upregulation of Orai1 in H_2O_2-treated rat MGCs (1 μM, 2 h) (Figures 3l and S2).

2.5 | Inhibition of SOCE/Orai protects retinal degeneration and reduces glial activation

We used retinal organotypic cultures for further investigation. Organotypic *in vitro* cultures allow the investigation of degenerative processes and the effects of neuroprotective treatments in this study. In organotypic cultures, the environment and conditions of retinas can be tightly controlled and manipulated, allowing for precise experimental conditions. This is not possible *in vivo*, where many confounding factors can influence experimental outcomes (Azadi et al., 2007; Belhadj et al., 2020; Caffé et al., 2001). To mimic RP, organotypic retinal cultures derived from *wt* mice were treated with Zaprinast for 48 h (Sahaboglu et al., 2013) (Figure 4a). Zaprinast is a well-known cyclic guanosine-monophosphate (cGMP) phosphodiesteras (PDE) inhibitor to target PDE6 specifically (Zhang et al., 2005). cGMP accumulation, due to a lack of PDE6, leads to photoreceptor death and retinal degeneration (Martínez-Fernández de la Cámara et al., 2013; Sahaboglu et al., 2013). Zaprinast treatment started at P15 and ended at P17. Next, the effect of Orai1 channels and the SOCE on the viability of photoreceptors were analyzed. To do so, the Zaprinast-treated retinas were exposed to 2-APB to inhibit SOCE/Orai1 (50 μM, 24 h) (Prakriya & Lewis, 2001; Yelshanskaya et al., 2021). TUNEL assay was then used to evaluate dead cells (Figure 4b-m). As results indicated, 2-APB treatment of Zaprinast-treated retinas reduced the number of TUNEL-positive cells and protected almost 50% of retinal cells (Figure 4n). However, treatment of healthy retinas with 2-APB alone increased TUNEL-positive cells. It is suspected that this result might be related to the dysregulation of cytosolic Ca^{2+} levels which eventually results in SOCE-dependent cytotoxicity and cell death.

It is known that gliosis is reflected by upregulation of GFAP protein in MGCs (Ekstrom et al., 1988). To ensure a process of gliosis in MGCs of retinal degeneration, we checked the effect of SOCE inhibition by 2-APB (24 h) treatment in Zaprinast-induced retinal degeneration (48 h) on the level of GFAP expression. Treatment of retinal explants with Zaprinast demonstrated an increased expression of GFAP. After SOCE/Orai1 inhibition by 2-APB, GFAP expression was
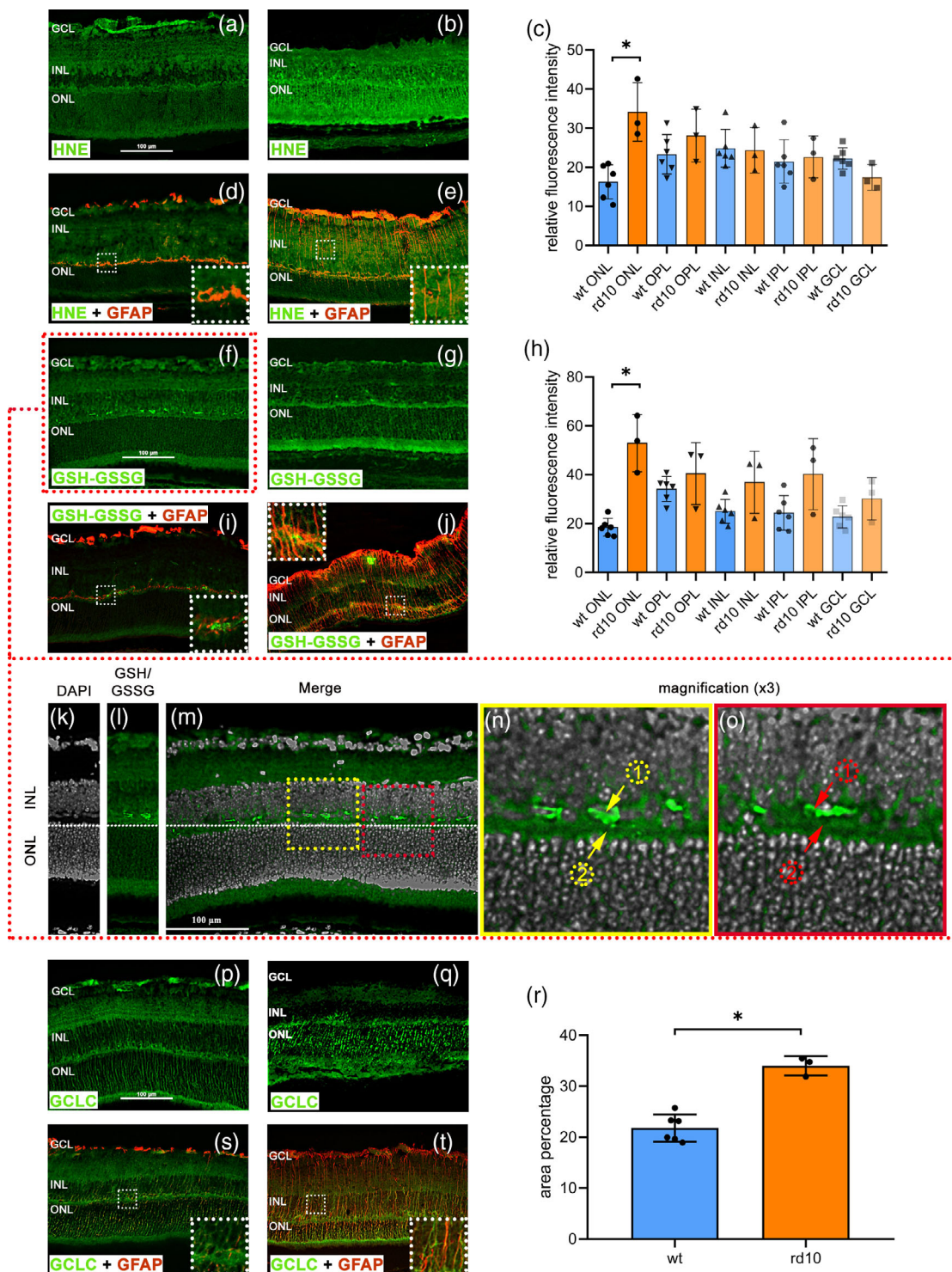
FIGURE 2 HNE, GSH-GSSG, and GCLC expression in *wt* and *rd10* mouse retinas. HNE expression showed immunoreactivity in *wt* retina (a) as well as *rd10* retina at P18 (b); quantitative analysis of fluorescence intensity levels of HNE in *wt* (blue bar, n = 6) and *rd10* (orange bar, n = 3) retinas in outer nuclear layer (ONL), outer plexiform layer (OPL), inner nuclear layer (INL), inner plexiform layer (IPL), and ganglion cell layer (GCL) (c); HNE colocalization with GFAP in *wt* (d) and *rd10* retinas (e); GSH and GSSG were expressed in *wt* retina (f) as well as *rd10* retina at P18 (g); quantitative analysis of the percentage of the retinal area occupied by the fluorescence of GSH and GSSG in *wt* (blue bar, n = 6) and *rd10* (orange bar, n = 3) retinas in ONL, OPL, INL, IPL, and GCL (h); GSH-GSSG colocalization with GFAP in *wt* (i) and *rd10* retinas (j); cells were stained with DAPI (k), GSH and GSSG (l), after merging, glutathione was expressed in the cytoplasm (m); three times magnified image of two retinal cells (n, o); The number 1 (yellow) indicated the DAPI-labeled cell nuclei and the number 2 (red) showed the cell cytoplasm; GCLC was expressed in *wt* retina (p) as well as *rd10* retina at P18 (q); quantitative analysis of the percentage of the retinal area occupied by the fluorescence of GCLC in *wt* (blue bar, n = 6) and *rd10* (orange bar, n = 3) retinas (r); GCLC colocalization with GFAP in *wt* (s) and *rd10* retinas (t); RPE, retinal pigment epithelium. *$p \leq .05$ indicates statistically significant difference, the Kolmogorov–Smirnov test.
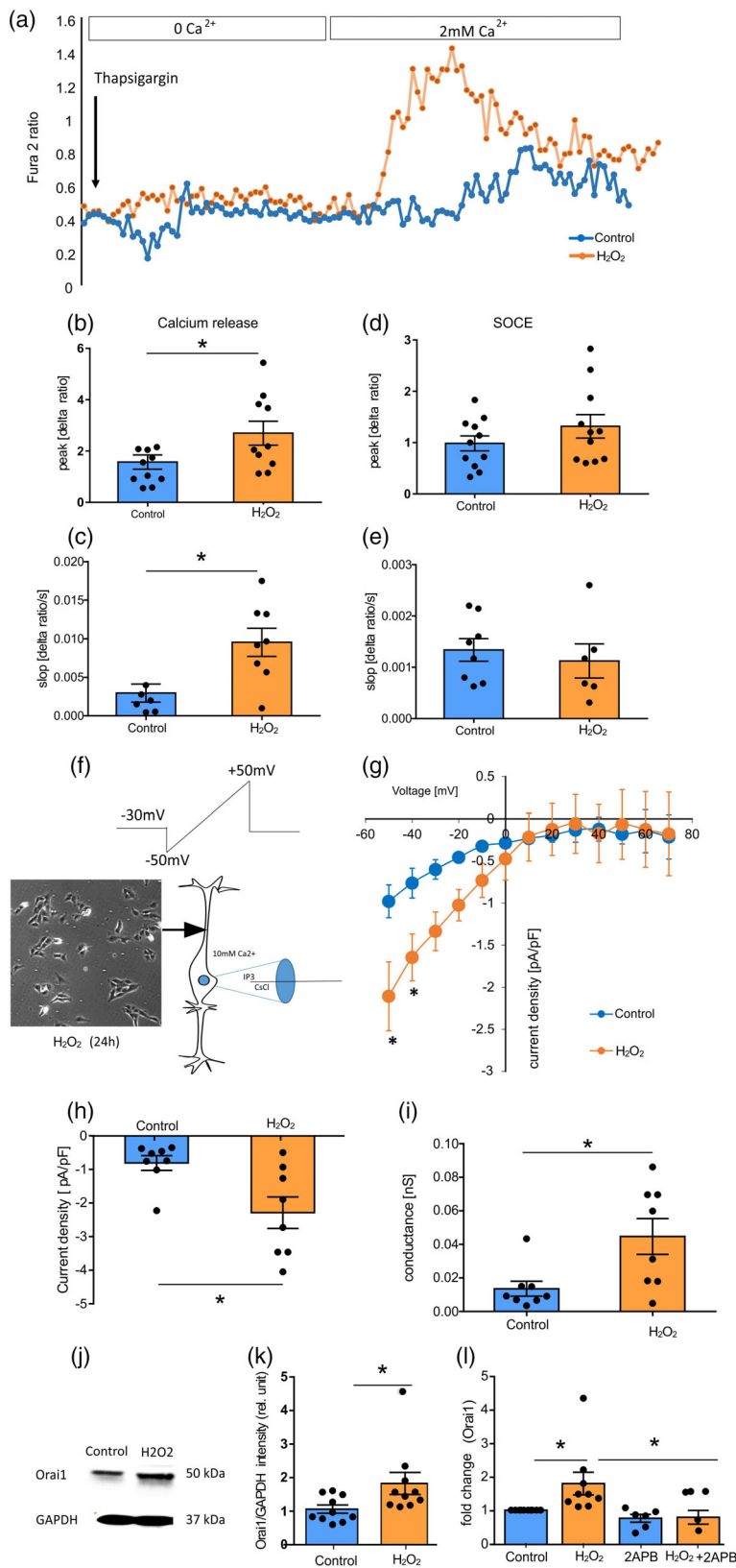
FIGURE 3 Intracellular Ca^{2+} release and SOCE as well as Ca^{2+} release-activated Orai channel, protein and RNA abundance of Orai1 in oxidative stressed rat MGCs. Fura-2 fluorescence-ratio tracings prior and after extracellular Ca^{2+} removal and addition of thapsigargin (1 μM), as well as in the presence of extracellular Ca^{2+} and thapsigargin in untreated (blue circles) and treated rat MGCs with H$_2$O$_2$ (2 h, 1 μM) to induce oxidative stress (orange circles) (a); arithmetic means (±SEM, $n = 11$ cells from 3 individuals) of slope (b) and peak (c) increase of Fura-2-fluorescence-ratio following the re-addition of extracellular Ca^{2+} in the presence of thapsigargin (1 μM) in MGCs without (blue bar) and with (orange bar) H$_2$O$_2$ (2 h, 1 μM) treatment (calcium release); arithmetic means (±SEM, $n = 11$) of peak (d) and slope (e) increase and decrease of fura-2-fluorescence-ratio following re-addition of extracellular Ca^{2+} in MGCs without (blue bar) and with (orange bar) treatment with H$_2$O$_2$ (2 h, 1 μM) (SOCE); The protocol of patch clamp experiment as voltage indicated (not to scale), whereby rat MGCs were held at 30 mV and ramp currents were injected for 200 ms from −50 to +50 mV (f); mean current–voltage (I/V) relationships of currents normalized to cell capacitance in untreated ($n = 7$) and treated rat MGCs with H$_2$O$_2$ (2 h, 1 μM) ($n = 8$) following the addition of 40 μM IP$_3$ (g); Mean peak current density ± SEM ($n = 7$) measured at −50 mV after the precondition potential to +50 mV in rat MGCs in untreated ($n = 7$) and treated rat MGCs with H$_2$O$_2$ (2 h, 1 μM) ($n = 8$) following the addition of 40 μM IP$_3$ (h); Mean whole-cell conductance of inward currents (±SEM, $n = 8$) calculated by linear regression of I/V curves shown in (i) between −50 and 0 mV; original western blot of Orai1 protein abundance in the absence or presence of H$_2$O$_2$ (2 h, 1 μM) in MGCs (j); Arithmetic means (±SEM, $n = 4$) of Orai1 protein levels in MGCs without (blue bars) or with H$_2$O$_2$ (2 h, 1 μM) treatment (orange bar) (k); arithmetic means (±SEM, $n = 4$) of normalized Orai1 transcript levels in rat MGCs without (blue bar) or with H$_2$O$_2$ (2 h, 1 μM) or 2-APB (10 μM) or H$_2$O$_2$ + 2-APB treatment (orange bar) using GAPDH mRNA as a reference (l); *$p ≤ .05$ indicates a statistically significant difference, unpaired t-test, and Kolmogorov–Smirnov test.
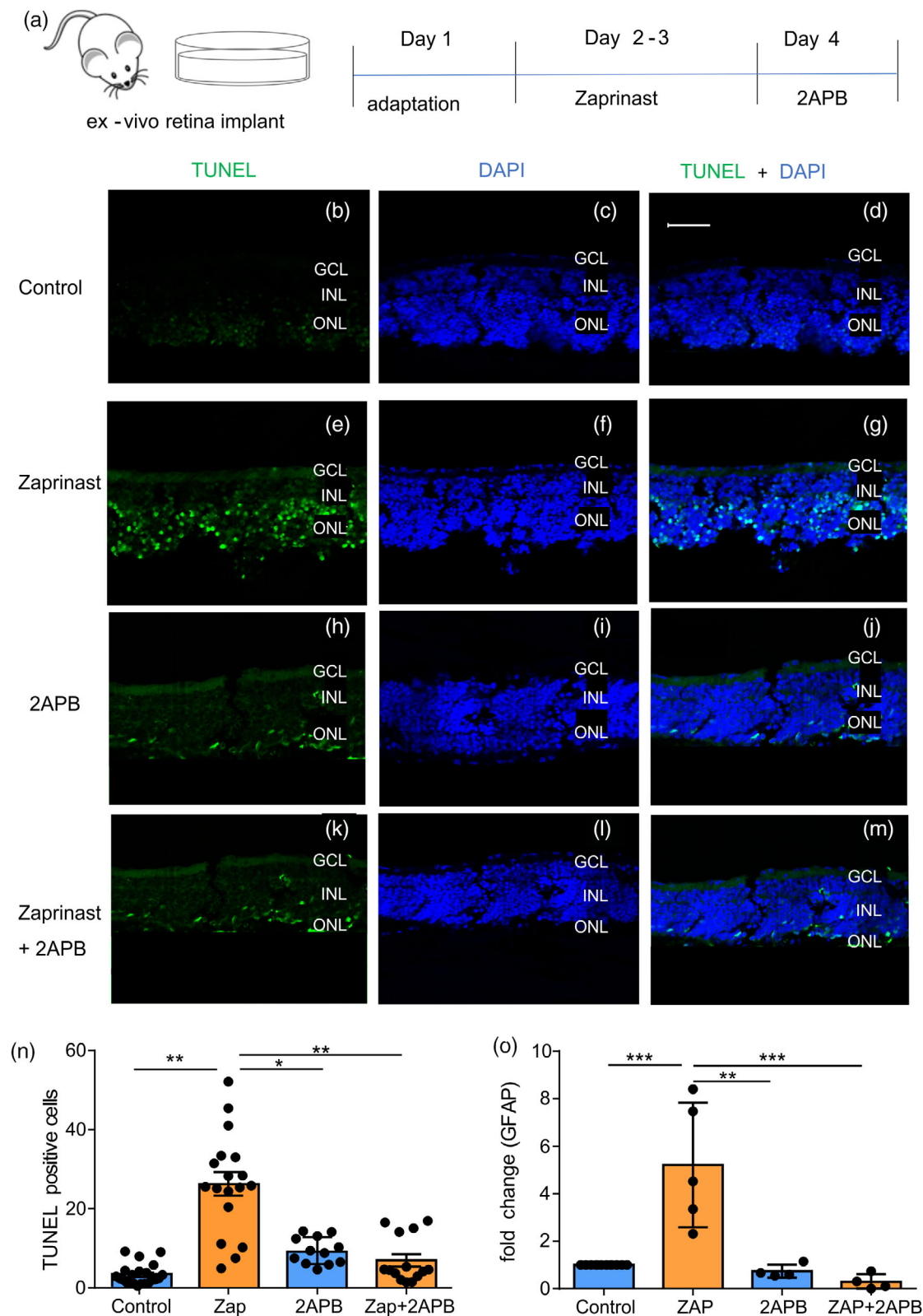
FIGURE 4 Effect of SOCE inhibition on the percentage of cell death and GFAP expression. (a–m) Immunostaining of organotypic retinal explant cultures from *wt* mice (P18) untreated (b–d); treated with Zaprinast, the PDE6 inhibitor (48 h) (e–g); 2-APB, SOCE inhibitor (50 μM, 24 h) (h–j); with Zaprinast +2-APB (k–m); DAPI (blue, first column), TUNEL assay (green, second column) and merged (third column), Scale bar (50 μm); Arithmetic means (±SEM, $n = 24$–43) of the quantified Tunnel-positive cells (n); Arithmetic means (±SEM, $n = 4$–9) of normalized GFAP transcript levels in homogenized retinal sections from *rd10* and *wt* mice (o); *$p \leq .05$, **$p \leq .01$, ***$p \leq .001$ indicate statistically significant difference, Kolmogorov–Smirnov test.

massively decreased in zaprinast treated retinas. This emphasizes the role of SOCE/Orai1 in the enhancement of gliosis and the activation of MGCs in retinal degeneration (Figure 4o).

2.6 | 2-APB mediates the closing of Orai1 by interacting with the Phe99 and Val102 hinge regions and blocking Ca^{2+} entry by binding to the selectivity filter

Using the ROBETTA (https://robetta.bakerlab.org) server in the comparative modeling mode (Raman et al., 2009; Song et al., 2013), the Orai1 channel was modeled for a better understanding of the inhibition mechanism of 2-APB. Initially, five models were developed and each of these five models was used in the ROSETTA static relax protocol (Table S1). A total of 100 conformers of the Orai1 channel were generated for each generated model (in total 500 conformers) and the conformer with the lowest total energy for each of the initial five models was selected as a representative structure. Before molecular docking, 100 ns all-atom molecular dynamics (MD) simulations were conducted for the relaxation of the structure (Figure S3). The 2-APB was prepared and docked to all selected models at their selectivity filter. For docking, the quantum-polarized ligand docking (QPLD) approach was used. An accurate definition of partial charges of docked ligands is crucial for both correct binding mode prediction and correct calculation of docking scores. Since QPLD uses ab initio charge calculations, partial charges were calculated with high accuracy. Next, these calculated charges were used in molecular docking. Results highlighted π-π stacking interactions of the phenyl groups of 2-APB with the phenyl side chain of Phe99 of Orai1. Another hydrophobic interaction was constructed with the Val102 residue and the ligand. Both Phe99 and Val102 residues have previously been reported as creating a "hinge" in STIM1-mediated opening and closing of the channel (Yamashita et al., 2017; Yeung et al., 2020). The complex structure was then merged with the lipid bilayer (dipalmitoylphosphatidylcholine DPPC). Afterward, a simulation box with counter ions, salt, water and a single calcium ion at the selectivity filter was used to proceed with (MD) simulations (Figure 5a). End-point MM/GBSA calculations were conducted for all five protein-ligand complexes (Table S1) and the lowest energy complex was used for further analyses. MD simulations of the aforementioned system revealed that upon binding of 2-APB, the water flow in the channel was substantially decreased. This result validated the modulatory effect of 2-APB on Orai1 channel activity (Figure 5b). Furthermore, contacts within the ligand and Phe99, Val102, and Glu106 residues were maintained for a whole 100 ns MD simulation (Figure 5c). More precisely, upon 2-APB binding at the Glu106 selectivity filter, the Glu106 coordination with incoming Ca^{2+} ions was hindered via hydrogen bonds between the amino group of 2-APB and the negatively charged oxygen of the glutamate residues of Orai1 (Figure 5d). The nature of the interactions between 2-APB and target residues can be summarized as mostly electrostatic interactions and hydrogen bonding between charged residues and π-π stacking (i.e., with Phe99)

or hydrophobic interactions (Figure 5e). Principal component analysis (PCA) of both the transmembrane domains TM1 (aa 88–105), TM2 (aa 120–140), TM3 (aa 174–194), and TM4 (aa 235–255) (Rosado et al., 2016), as well as the full-length Orai1 in apo and holo forms were conducted (Figure 5f). Then, the first 10 eigenvector indices were plotted. It has been reported previously (Jarmula et al., 2019) that these 10 indices of mobility were enough to demonstrate the divergence of motion across the simulation. The PCA analysis reported the decrease in structural mobility of 2-APB bound Orai1 when compared to its apo form. Furthermore, the transmembrane domains (Figure 5f; top) and full-length protein (Figure 5f) PCA showed correlated absolute eigenvalue magnitudes (Zhang et al., 2005; Sahaboglu et al., 2013).

3 | DISCUSSION

The present study uncovers a novel regulation of Orai1 as an important determiner of intracellular Ca^{2+} concentrations in the MGCs in retinal degeneration. Orai1 is thereby upregulated in the MGCs during photoreceptor degeneration induced by oxidative stress in _rd10_ mice. Therefore, inhibition of SOCE/Orai1 by 2-APB preserves photoreceptors in degeneration process. We modeled the Oria1 structure for the first time, and the efforts suggest the structural and dynamical aspects of 2-APB to the target structure of Orai1. This is an approach to find therapeutic pathways for photoreceptor degeneration in RP by focusing on MGCs.

In our study, we have shown a higher expression of Orai1 in the MGCs of _rd10_ retinas. It has been previously reported that mouse MGCs massively express Orai1 and stromal interaction molecules (STIM) 1 and 2 in glial end-feet within the OPL and RGC layers (Molnár et al., 2016). The STIMs work in cooperation with Orai1 to form pore subunits of the CRAC channel (Liou et al., 2005). Orai1 upregulation in MGCs may utilize the canonical STIM mechanism in _rd10_ retinas. The Orai1 mechanism may function in co-occurrence or cooperation of other components of the MGCs' membrane, including Ca^{2+} ATPases, Ca^{2+} release channels, aquaporin 4 (AQP4), SERCA2, and Kir 4.1 (Chen et al., 2014; Jo et al., 2015). In our study, the double labeling with the active MGCs marker, GFAP, colocalized with Orai1 channels, showed that Orai1 expression was higher in the ONL, INL, and GCL of _rd10_ retinas. The Orai1 expression was pronounced in the GCL where the end-foot of MGCs was placed in _rd10_ retinas. Alteration of cytosolic Ca^{2+} activity ([Ca^{2+}]$_i$) might be triggered by SOCE (Lang et al., 1991), which in turn may induce rapid Ca^{2+} entry mediated by Orai1 channels (Parekh, 2017). This Ca^{2+} entry conducts different cellular functions (Berridge et al., 2003; Parekh & Penner, 1997) including entry into the S and the M phases of the cell cycle (Taylor et al., 2008) and cell survival (Heise et al., 2010; Parkash & Asotra, 2010). In contrast, sustained increases of [Ca^{2+}]$_i$ activity induce apoptosis in a variety of cell types (Fang et al., 2008; Green & Reed, 1998; Lang & Hoffmann, 2012). Thus, cell survival or death relies upon a sensitive harmony between activators and inhibitors of Ca^{2+} entry. Therefore, it is tempting to hypothesize that
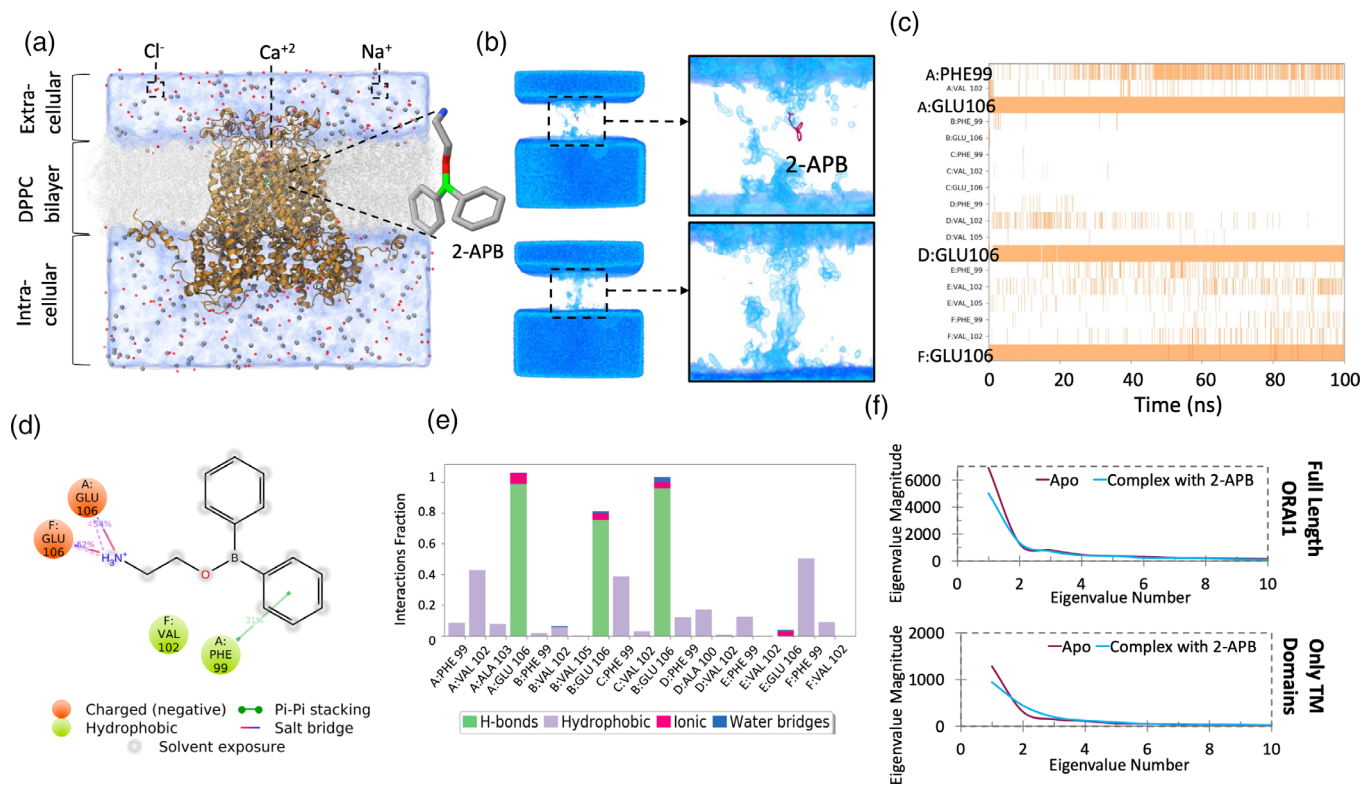
FIGURE 5   2-ABP modulates the Orai1 pore opening via binding to the Glu106 selectivity filter and interacting with the Phe99/Val102 hinge region. Simulation box with 2-APB bound Orai1 channel embedded in water, counterions and lipid bilayer (a); Water map of apo form (bottom) and 2-APB bound (top) Orai1 channel (b); Protein-ligand interactions throughout the 100 ns MD simulations; Panel represents the formed (marked with orange) and broken (left blank) interactions between the protein and ligand for the duration of the 100 ns simulations (c); 2D interaction map of 2-APB with protein residues (d); Interaction fractions and the types of interactions during the 100 ns simulations are depicted (e); Principal component analysis (PCA) for 2-APB bound Orai1 and apo form; Transmembrane domains of Orai1 (top) and full-length Orai1 (bottom) were considered separately. Magnitudes of the first 10 eigenvalues are plotted (f).

throughout the retinal degeneration in *rd10* mice, Orai1 expression is in part upregulated which may then activate photoreceptor death.

Oxidative stress is often connected with retinal degenerative diseases including RP, age related macular degeneration (AMD) and diabetic retinopathy (DR). Oxidative stress leads different responses in MGCs including rapid dedifferentiation, enhanced proliferation, reduced glutamate uptake, collapsed mitochondrial function, and glutathione synthesis (Abrahan et al., 2009; Toft-Kehler et al., 2016). MGCs could have protective or detrimental effects on retinal neurons when introducing oxidative stress. Our results confirmed both possibilities in MGCs of *rd10* mice. Our observation demonstrated increased HNE, the natural by-product of lipid peroxidation in response to oxidative stress in *rd10* retinas. HNE is a reactive aldehyde formed from the nonenzymatic oxidation of n-6 polyunsaturated fatty acids and is cytotoxic by itself (Tanito et al., 2005). This result is consistent with previous reports (Tanito et al., 2005; Trachsel-Moncho et al., 2018). Additionally, GSH is a peptide that also protects against oxidative stress and exists in the form of reduced thiol (GSH) and oxidized disulfide (GSSG). Its synthesis involves two enzymatic steps, the first one being the limiting step, and it is catalyzed by glutamate cysteine ligase (GCL) (Zhong et al., 2013). In this study, we have examined the expression of the catalytic subunit of this enzyme. Our

results, in agreement with previous studies (Sánchez-Vallejo et al., 2016), showed that GSH synthesis and GCLC colocalized with GFAP were upregulated in the rd10 retinas. This upregulation might be an attempt to fight against oxidative stress.

Similar to MGCs from retinal degeneration *rd10* mice, we found that H_2O_2-induced oxidative stress in rat MGCs led to an increasing peak and slope of Ca^{2+} entry as well as Orai current and expression. In line with previous studies, it has shown that cell death by oxidative stress is paired with increased levels of detrimental Ca^{2+} influx specifically through Orai1 in a mouse hippocampal cell line (Henke et al., 2013). SOCE is sub-served by synergistic activation of TRPC1 and Orai1 channels in adult native MGCs. Orai1 expression of MGCs that protect retinal neurons is suspected to buffer Ca^{2+} homoeotic (Molnár et al., 2016). SOCE is itself sufficient for the initiation and subcellular propagation of Ca^{2+} waves in mouse MGCs that are independent of ATP release and activation of P_2X and P_2Y receptors (Phuong et al., 2016). The intraocular pressure-induced gliotic response is facilitated in the absence of TRPC1 (Molnár et al., 2016). We discovered an upregulation of the SOCE-triggered Orai1 function in rat MGCs under H_2O_2-induced stress. It has been revealed that TRPC1 insertion into the plasma membrane relies on the Orai activation (Chen et al., 2014; Vaca, 2010), and Orai plays as a regulatory

element of the TRPC/STIM pore (Liao et al., 2014) although replenishment of the ER Ca^{2+} pool is crucial for keeping up MGCs' excitability and capacity. Nevertheless, the character of ion channels, for example, SOCE/Orai and SOCE/TRPC and their impact on Ca^{2+} homeostasis, function, and pathology of retinal degeneration remain unclear. Our results have indicated that oxidative stress due to retinal degeneration causes activation of SOCE/Orai.

As photoreceptor death and increased oxidative stress have been paralleled by increased Ca^{2+} entry through the Orai1 channel in MGCs in our study, we can hypothesize that inhibition of SOCE and Orai1 may prevent photoreceptors in degeneration process. Here, we mimicked retinal degeneration by using Zaprinast and we then treated with 2-APB. Our results reflected that 2-APB abrogated the effect of Zaprinast and prevented photoreceptors during the course of degeneration. This cell survival could be an effect of decreased Ca^{2+} entry through Orai1 channels after its inhibition. This deserves further investigation, as inhibition of SOCE with 2-APB decreased GPAF expression under retinal degeneration. Decreased Orai1 activity might affect a reactive gliosis of MGCs, resulting release of a range of factors or preventing glutamate neurotoxicity and so protecting neurons from cell death. As our data indicated that inhibition of store-operated Ca^{2+} channels prevented cell death, this inhibition may interfere with retinal Ca^{2+} homeostasis and the ability of MGCs to support retinal neurons and thus protect retina from neurodegeneration.

Molecular dynamics simulations of the 2-APB complexed Orai1 channel revealed that water flow through the channel substantially decreased upon binding of the ligand (Figure 5b). Furthermore, in silico investigation also revealed the binding mechanism of 2-APB at the selectivity filter where its positively charged amino group interacted with the negatively charged side chain of the glutamate residues (i.e., Glu106) from chains A and F. This interaction fixed the ligand in the docking region and allowed for Phe99 and Val102 sidechain interactions with the phenyl groups of 2-APB. Root mean square fluctuation (RMSF) plots showed the stabilization of the respective chains of (Figure S4). As previously uncovered (Yamashita et al., 2017; Yeung et al., 2020), Phe99 and Val102 form the crucial hydrophobic "hinge" residues that play a critical role in the opening mechanism of Orai1. Our findings suggest that 2-APB is a modulator of the hinge via hydrophobic interactions (i.e., Val102) as well as π-π stacking interaction of the aromatic ring of Phe102 that pull the hydrophobic hinge residues inwards and closes the pore (Supplementary data, Movie 1). Furthermore, the exploration of principal component (PC) space of Orai1 in holo and apo forms revealed that both transmembrane domains and full-length Orai1 correlated to structural mobility with respect to their ligand-bound and apo forms. Binding of the ligand to the channel decreased the mobility (structural fluctuations) of both the whole structure and transmembrane domains as shown the pattern of the amplitudes (eigenvalues) associated with eigenvectors (Zhang et al., 2005; Sahaboglu et al., 2013).

Orai1 inhibitors are important tools to understand the role of SOCE in different disease progressions, including retinal diseases. Different Orai1 inhibitors have been developed and some of them have now reached clinical trials for various indications such as rheumatoid,
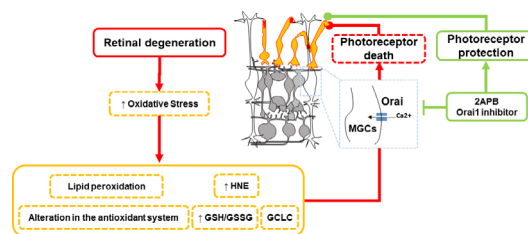
FIGURE 6 Summary of the study. Oxidative stress is an important pathological mechanism in the rd10 retinal degeneration. HNE expression, a product of lipid peroxidation, is increased in the outer nuclear layer of rd10 retinas. GSH-GSSG, the major intracellular antioxidant, GCLC, and the rate-limiting enzyme in the de novo synthesis of GSH are increased in RP in an effort to deal with increased oxidative stress (yellow). Inducing oxidative stress in Müller glial cells (MGCs) results in increasing store-operated Ca^{2+} entry (SOCE) and Ca^{2+} release. Inhibition of SOCE and its major component, Orai1 channel, by 2-APB in MGCs protects photoreceptors from degenerating (oxidative stress process = yellow; degenerative pathway = red; protective pathway = green; white cells = MGCs; orange cells = photoreceptors; gray = other retinal cells; blue = Orai channels).

psoriatic arthritis, multiple sclerosis (Fragoso & Brooks, 2015), severe plaque psoriasis, acute pancreatitis, asthma, and COVID-19-associated severe pneumonia (Miller, 2020; Stauderman, 2014). These studies, together with our results, highlight the Orai1 channel inhibitors' potential and tolerability in a therapeutic capacity for retinal diseases such as RP and AMD. In addition to available data, rapidly increasing knowledge about the implications of Orai1 in different disease pathologies has potential for developing novel therapeutic tools. In the future, current data could facilitate translation into clinical studies for retinal degenerative diseases. Further studies are required to fully elucidate the Orai1-dependent pathways in retinal degeneration processes such as the side effects of Orai1 inhibitors; changes in calcium homeostasis in non-target cells; possible off-target effects on other ion channels or enzymes; and the systemic consequences of in vitro and in vivo approaches. This information is crucial to ensure the safety and efficacy of Orai1 inhibitors in clinical applications for retinal diseases.

In conclusion, SOCE/Orai1 of MGCs is responsible in part for the photoreceptor death caused by oxidative stress that may directly connected to retinal degeneration and leads the pathological status in RP (Summary; Figure 6). Therefore, it can be concluded that Orai1 and SOCE inhibition may present therapeutic possibilities and be a valuable tool for treatment of retinal degeneration. Our results shown here may provide a potential clinical study for exploring the functional mechanism of Orai1 in the course of RP.

4 | METHODS

4.1 | Animals

All animal experiments were conducted according to the German law for the welfare of animals and approved by the authorities of the state

of Baden-Württemberg and Sachsen. Experiments were performed with retina from P15-P18 female and male gene-targeted mice lacking functional PDE6 (rd10) and in age- and sex-matched wt (Jackson Lab). The mice have free access to water and control food in the standard cages according to German law.

4.2 | Mouse Müller glial cells

Mouse Müller cells were used from retinas of rd10 and wt (Jackson Lab). Müller cells were isolated using papain- and DNase I-containing solutions, as described previously (Puro et al., 1989). The cell suspensions were stored at 4°C (up to 10 h) before performing experiments in DMEM medium supplemented with 10% FCS and 1% penicillin–streptomycin.

4.3 | Immunofluorescence

The eyes of the animals were enucleated after they were euthanized sacrificed with CO_2. Then, eyecups were immersion fixed for 1 h at room temperature in 4% PFA (Poysciences, Warrington, PA) in a 0.1 M phosphate buffer (PB, pH 7.4), containing 0.2 M sucrose. After washing in PB, the eyes were cryoprotected by immersion in graded sucrose including 10%, 20%, and 30% in PB. The eyes were then immersed in a medium for tissue-freezing (Jung, Leica Instruments, Heidelberg, Germany). Vertical sections (12 μm) were cut on a Leica CM3050S Microtome (Leica Biosystems, Wetzlar, Germany), air-dried at 37°C for 1 h, and stored at −20°C until use. Frozen sections from fixed tissue were air-dried for 30–60 min at 37°C.

Retinal sections were rinsed in PBS and preincubated in a blocking solution (10% normal goat serum, 1% bovine serum albumin (BSA) and 0.1% (Orai1 analysis) or 0.3% (oxidative stress markers analysis) Triton X in PBS) for 1 h at room temperature (Orai1 analysis) or 4°C (oxidative stress markers analysis). Retinal sections were washed three times for 10 min with PBS-Triton 0,3% and incubated with primary antibodies overnight at 4°C: Orai1 (1:1000, 13130-1-AP, Proteintech), rabbit anti-HNE antiserum (1:100, HNE11-S, Alpha Diagnostic); Rb X Glutathione (1:100, AB5010, Merck Millipore, catalytic subunit of the enzyme glutamate cysteine ligase (1:100, ab240379, Abcam), GFAP (1:100, G-3893, Sigma-Aldrich) or (1:500, Z0334, Dako). Subsequently, sections were rinsed in PBS and incubated with Alexa fluor-488 conjugated secondary antibody (1:250–1:750, A11008, Invitrogen) or Texas Red Conjugated Avidin (1:200, A820, Molecular Probes Inc). After washing sections with PBS, they were mounted in a Vectashield mounting medium with DAPI (Vector, Burlingame, CA).

4.3.1 | Orai1 analysis

A Zeiss Axiocam digital camera and the Zeiss Axiovision 4.7 software were used to capture images. An image of each section was taken by Zeiss Imager Z1 Apotome microscope. The Corel Draw X3 software

package was used to enhance the contrast and colors of images. The percentages of positive cells were assessed and calculated in a blinded fashion as reported previously (Sahaboglu et al., 2016). For each animal (wt and rd10), three fields of view at 20× magnification in central retinal areas (in proximity to the optic nerve) were analyzed and at least three sections were quantified. At least three different animals were analyzed for each condition and genotype. For quantification of results, Image J was used to measure the fluorescence intensity of Orai1 expression in wt and rd10 retinas.

4.3.2 | Oxidative stress markers analysis

Images were taken with a Nikon DS-Fi1 camera attached to a Leica DM 2000 microscope. The Leica application Suite version 2.7.0 R1 program (Leica Microsystems SLU, Barcelona, Spain) was used. ImageJ Fiji version 1,52p software was used to quantify data. To evaluate changes in oxidized GSH and GCLC enzymes, the percentage of area occupied by these proteins was determined. Lastly, in the case of hydroxynonenal expression (HNE), pixel-green intensity was quantified.

4.4 | Rat Müller cell line

Immortalized rat retinal Müller cells (rMC-1) (ABM) were cultured in DMEM medium supplemented with 10% FCS and 1% penicillin–streptomycin. The incubation took place at 37°C and 5% CO_2 in the incubator.

4.5 | Ca^{2+} measurements

Fura-2 fluorescence was taken as a Ca^{2+} indicator to measure the cytosolic Ca^{2+} activity $[Ca^{2+}]_i$, as described previously (Yan, Zhang, et al. 2016; Yan, Hosseinzadeh, et al. 2016). For this purpose, MGCs were incubated with Fura-2/AM (2 μM, Invitrogen, Goettingen, Germany) for 20 min at 37°C. At 340 and 380 nm alternatively, MGCs were excited through an objective (Fluor 40×/1.30 oil) of an inverted fluorescence microscope (Axiovert 100, Zeiss, Oberkochen, Germany) and at 505 nm the emitted fluorescence intensity was recorded. For acquiring data, we used Metafluor software (Metafluor, Universal Imaging, Downingtown). $[Ca^{2+}]_i$ activity was evaluated from the ratio of 340 nm/380 nm. To record SOCE function, a sequence change of the extracellular solution was done: first, extracellular Ca^{2+} removal and subsequent Ca^{2+} re-addition in the presence of Thapsigargin (1 μM, Invitrogen). For analyzing Ca^{2+} entry, the slope (delta ratio/s) and peak (delta ratio) were calculated following re-addition of Ca^{2+}.

Bath solution was composed of (in mM): 125 NaCl, 5 KCl, 1.2 $MgSO_4$, 2 $CaCl_2$, 2 Na_2HPO_4, 32 HEPES, 5 glucose, pH 7.4. For Ca^{2+}-free conditions, the Ca^{2+}-free solution was composed of (in mM): 125 NaCl, 5 KCl, 1.2 $MgSO_4$, 2 Na_2HPO_4, 32 HEPES, 0.5 EGTA, 5 glucose, pH 7.4.

4.6 | Whole-cell patch clamp

Patch-clamp experiments were performed in voltage clamp (fast-whole-cell mode) either in rat Müller cells or isolated mouse Müller cells from mouse retina, at room temperature. The currents of channels were recorded by an EPC-9 amplifier (Heka, Lambrecht, Germany) using Pulse software (Heka) and an ITC-16 Interface (Instrutech, Port Washington, NY). I_{CRAC} were recorded with 200 ms voltage ramps from -50 to $+50$ mV (Figure 3f). The currents at the very beginning of each experiment immediately after reaching the whole-cell mode were defined as leak currents and subtracted. For recording the currents, an acquisition was adjusted to a frequency of 10 kHz with a 3 kHz low-pass filter. MGCs were super-fused with a bath solution containing (in mmol/l): 140 NaCl, 5 KCl, 10 CaCl$_2$, 20 glucose, 10 HEPES/NaOH, pH 7.4. The internal solution (patch clamp pipette) was (in mmol/l): 120 CsCl, 35 NaCl, 10 EGTA, 10 HEPES/CsOH, 0.04 inositol 1, 4, 5-trisphosphate (Ins $(1,4,5)$P$_3$, Enzo Life Sciences), pH 7.4. The liquid junction potential ΔE between the CsCl-based pipette and the NaCl-based bath solutions was estimated according to Barry and Lynch and approached 1 mV. For ΔE, the data was not corrected.

4.7 | Western blot

Protein abundance of Orai1 and GAPDH was determined by western blotting. To this end, MGCs were seeded in a six-well plate. 200 μL of ice-cold RIPA lysis buffer (Thermo Fisher Scientific) was applied to isolate protein. Then, by using a spatula, the cells were scraped from the plate and placed in an Eppendorf tube. Protein was solubilized in a sample buffer at 90°C for 10 min. The proteins were separated by a 10% SDS-PAGE in a glycine–tris buffer and then electro-transferred onto nitrocellulose membranes overnight at a voltage of 25 V. After blocking with 5% BSA in TBST (a mixture of tris-buffered saline (TBS) and Tween) at room temperature for 1 h, the membranes were incubated with primary anti-rabbit Orai1 antibody (1:1000, 13,130-1-AP, proteintech) and anti-GAPDH antibody (1:2000, #2118s, Cell Signaling) at 4°C overnight. The blots were then washed with TBST and incubated with a secondary anti-rabbit antibody conjugated with horseradish peroxidase (1:2000, Cell Signaling) for 1 h at room temperature. Protein bands were detected after additional washes (TBST) with an ECL detection reagent (Vilber, Germany) and quantified with Evolution-Capt Edge Software. Protein-Marker VI (Peqlab, Erlangen, Germany) was used for assigning the right size of targeted proteins.

4.8 | Quantitative real-time PCR

Transcript levels of Orai1, GFAP and housekeeping glyceraldehyde 3-phosphate dehydrogenase (GAPDH) were determined by real-time quantitative PCR (RT-PCR). Total RNA of MGCs or homogenized retinas was extracted in TriFast (Peqlab, Erlangen, Germany) according to the manufacturer's instructions. Then RNA concentrations were measured by Nanodrop 2000 Spectrophotometer (Thermo Scientific).

Amplification of the respective genes was set up in a total volume of 20 μL using 15 ng of RNA. 600 nM forward and reverse primers and the Qiagen OneStep RT-PCR Kit were utilized for amplification according to the manufacturer's instructions.

The following primers were used for amplification (5′ – >3′ orientation):

GAPDH	Forward: AGTGCCAGCCTCGTCTCATA
	Reverse: GGTAACCAGGCGTCCGATAC
Orai1	Forward: GCCAGAGTTACTCCGAGGTG
	Reverse: ATCGCTACCATGGCGAAGC
Orai2	Forward: GTGGGTCTCATCTTCGTGGT
	Reverse: CCACCTGTAGGCTTCTCTCG
Orai3	Forward: GCCCAGCTTTAGACTGTTGC
	Reverse: CTGAGCAGGAATTTGGCTTC
GFAP	Forward: CAAGCACGAGGCTAATGACT
	Reverse: CAATTTCCTGTAGGTGGCGA

The specificity of RT-PCR products was confirmed by the analysis of a melting curve. RT-PCR amplifications were performed on a Rotor-Gene Q Real-Time Thermocycler (QIAGEN, Stockach, Germany) and all experiments were done in duplicate. The house-keeping gene GAPDH was amplified to standardize the amount of the sample RNA.

4.9 | Retinal explant cultures

The isolated retinas from mice (Mus musculus C57BL) were cultured into a culture membrane insert (Millipore, Carrigtwohill, Cork, Ireland; PIHA03050) with the photoreceptor side down. The inserts were transferred into six-well plates. Explants were incubated in R16 medium with supplements at 37°C in a humidified 5% CO$_2$ incubator. The cultures were started at P15 and after 2 days of cultural adaptation, they were treated at P17 and finalized at P19. Retinal organotypic explants were treated with 100 μM Zaprinast for 48 h to induce retinal degeneration. Where indicated, explants were treated with 50 μM 2-APB for 24 h. After treatment with Zaprinast and/or 2-APB, cultures were either fixed for TUNEL assay or RNA-isolated.

4.10 | TUNEL assay and cell counting

Terminal deoxynucleotidyl transferase dUTP nick end labeling (TUNEL) assay was performed using an in-situ cell death detection kit (Fluorescein, Roche Diagnostics GmbH, Mannheim, Germany) to detect dying cells. For negative controls, sections were incubated with terminal deoxynucleotidyl transferase enzymes omitted from the labeling solution; for positive control sections, they were pre-treated for 30 min with DNAse I (Roche, 3 U/mL) in 50 mM Tris–HCl, pH 7.5, 1 mg/mL BSA to induce DNA strand breaks. Positive control stained all nuclei in all layers of the retina, whereas negative control gave no staining at all.

4.11 | Reagents and drugs

2-APB and MRS-1845 were purchased from Tocris Bioscience and GSK-7975A, Zaprinast and hydrogen peroxide from Sigma-Aldrich.

4.12 | Statistics

Data are expressed as arithmetic means ± SEM. Statistical analysis was performed using GraphPad Prism 6 software (GraphPad Software, La Jolla, CA); for one-to-one group comparisons, Student's t-test (non-parametric test) was used; for multiple group analyses, one-way ANOVA (non-parametric test) and Kolmogorov–Smirnov as post hoc tests were used. $P < .05$ was considered statistically significant.

4.13 | Molecular simulations

4.13.1 | Protein modeling and preparation

The homo-hexameric human Orai1 3D atomistic models were generated using the Robetta (https://robetta.bakerlab.org) in the comparative modeling mode (Raman et al., 2009; Song et al., 2013). In this module, the given sequence was aligned with existing crystal structures (i.e., multiple sequence alignment), and the 3D conformation of the five model proteins was assembled. For each of the models, 100 conformers (in total 500) were generated along with their calculated total energies using the Rosetta software, and the conformation with the lowest total energy was used as a representative structure. A calcium ion, aligned from the drosophila Orai1 model (PDB: 4HKS) (Hou et al., 2012) was inserted in the pore region at 4.65 Å distance to the Glu106 residues of the selectivity filter in our model. Protein preparation was done using the Protein Preparation module of the Maestro molecular modeling package (Madhavi Sastry et al., 2013). Zero-bond orders were assigned between the Ca^{+2} and the Glu106 residues of each chain. Protonation states of the residues at the target protein and hydrogen bond assignment were performed using the PROPKA3 server (Olsson et al., 2011) at 7.4 physiological pH and restrained minimization was applied until the convergence of the heavy atoms to 0.15 Å. The OPLS3e force field (Harder et al., 2015) was used for all energy minimizations.

4.13.2 | Ligand preparation

The ligand, (2-APB) was prepared using the LigPrep module of the Maestro molecular modeling package. The OPLS3e force field (Harder et al., 2015) was used. Possible ionization states were generated at pH 7.4 $+/-0.5$ using the Epik module (Shelley et al., 2007). The output ligand with the lowest energy was later submitted to the Jaguar module (Klicic Klicic et al., 2002) of the Maestro molecular modeling package for Ab initio quantum mechanical geometry optimization. The density functional theory (DFT) based method at B3LYP/6-31G** basis set was utilized.

4.13.3 | Molecular docking

Molecular docking was conducted using the QM-polarized ligand docking (QPLD) module (Cho et al., 2005) of the Maestro molecular modeling package. The centroid of the Glu106 of all chains was chosen for the box center of the docking grid box. Partial charges of the atoms at the 2-APB calculated by the QM were used at the docking. Initial docking was performed with standard precision (SP) and final docking was performed at extra precision (XP) mode. The resulting molecule with the highest docking score (in absolute values) was used in all-atom MD simulations.

4.13.4 | Molecular dynamics simulations

PPM2.0 web server (Lomize et al., 2012) (https://opm.phar.umich.edu/ppm_server) was used for the alignment of the membrane with the channel. The membrane system was used as a template for the setup of the MD simulations. The Orai1 homo-hexamer (apo form) and the holo form (i.e., Orai1:2-APB complex) were merged in a DPPC bilayer. The systems were then solvated with the TIP3P water model. Counter ions and 0.15 M concentration of salt were added to neutralize the system. All-atom simulations were conducted using Desmond. The NPT ensemble was used and the system was kept at constant temperature and pressure with the Nose-Hoover thermostat (Hoover, 1985) and Martyna-Tobias-Klein barostat (Martyna et al., 1998) at 310 K and 1.01325 bar, respectively. The particle mesh Ewald (PME) summation method was used to calculate the long-range electrostatic interactions of the periodic boundary conditions. The RESPA (Tuckerman et al., 1992) multi-time step integration scheme was used, and the time steps were varied for interaction type. Finally, 100 ns production simulations were conducted for apo and holo systems.

4.13.5 | MM/GBSA calculations

Binding free energies of the 2-APB bound-Orai1 systems were calculated using the Prime-MM/GBSA module (Jacobson et al., 2004) of the Maestro molecular modeling package. The protein-ligand complexes were extracted and solvated in the implicit solvent model VSGB 2.0 (Hoover, 1985; Li et al., 2011) using the OPLS3e force field (Harder et al., 2015). Average MM/GBSA scores were calculated for each saved trajectory.

4.13.6 | Water density map analysis

Water density maps were created using the *maptide* module from GROmaps (Briones et al., 2019). Water volume visuals were created using Pymol (Schrödinger LLC 2010).

4.13.7 | Principal component analysis

Principal component analysis of the conformations adopted by the 3D Orai1 structure during the 100 ns MD simulations was computed using the Bio3D library (Grant et al., 2006) in R Studio. Full-length PDB structure and transmembrane domains were calculated separately for apo form and holo complex with 2-APB.

AUTHOR CONTRIBUTIONS
Basma Sukkar, Ayse Sahaboglu, Lalehan Oktay, Aylin Moayedi, Shima Zenouri, Tamer Al-Maghout, Antolin Cantó, María Miranda, Serdar Durdagi, and Zohreh Hosseinzadeh performed experiments; Zohreh Hosseinzadeh designed the study, Basma Sukkar, Lalehan Oktay, Serdar Durdagi, and Zohreh Hosseinzadeh drafted the manuscript. All authors corrected and approved the final version of the manuscript.

CONFLICT OF INTEREST STATEMENT
The authors declare no conflicts of interest.

DATA AVAILABILITY STATEMENT
Authors follow the rule of data transparency. All authors have made sure that all data and materials, including software applications, support their published claims and comply with field standards.

ORCID
Zohreh Hosseinzadeh https://orcid.org/0000-0003-3407-7754

REFERENCES
Abrahan, C. E., Insua, M. F., Politi, L. E., German, O. L., & Rotstein, N. P. (2009). Oxidative stress promotes proliferation and dedifferentiation of retina glial cells in vitro. *Journal of Neuroscience Research*, *87*, 964–977.

Azadi, S., Johnson, L. E., Paquet-Durand, F., Perez, M. T. R., Zhang, Y., Ekström, P. A. R., & Van Veen, T. (2007). CNTF + BDNF treatment and neuroprotective pathways in the rd1 mouse retina. *Brain Research*, *1129*, 116–129.

Belhadj, S., Tolone, A., Christensen, G., das, S., Chen, Y., & Paquet-Durand, F. (2020). Long-term, serum-free cultivation of organotypic mouse retina explants with intact retinal pigment epithelium. *Journal of Visualized Experiments*, *165*, e61868. https://doi.org/10.3791/61868

Berridge, M. J., Bootman, M. D., & Roderick, H. L. (2003). Calcium signalling: Dynamics, homeostasis and remodelling. *Nature Reviews. Molecular Cell Biology*, *4*, 517–529.

Bird, G. S., DeHaven, W. I., Smyth, J. T., & Putney, J. W. (2008). Methods for studying store-operated calcium entry. *Methods*, *46*, 204–212.

Briones, R., Blau, C., Kutzner, C., de Groot, B. L., & Aponte-Santamaría, C. (2019). GROmaps: A GROMACS-based toolset to analyze density maps derived from molecular dynamics simulations. *Biophysical Journal*, *116*, 4–11.

Caffé, A. R., Ahuja, P., Holmqvist, B., Azadi, S., Forsell, J., Holmqvist, I., Söderpalm, A. K., & Van Veen, T. (2001). Mouse retina explants after long-term culture in serum free medium. *Journal of Chemical Neuroanatomy*, *22*, 263–273.

Chen, M., Križaj, D., & Thoreson, W. B. (2014). Intracellular calcium stores drive slow non-ribbon vesicle release from rod photoreceptors. *Frontiers in Cellular Neuroscience*, *8*, 20.

Cho, A. E., Guallar, V., Berne, B. J., & Friesner, R. (2005). Importance of accurate charges in molecular docking: Quantum mechanical/molecular mechanical (QM/MM) approach. *Journal of Computational Chemistry*, *26*, 915–931.

Eastlake, K., Luis, J., & Limb, G. A. (2019). Potential of Müller glia for retina neuroprotection. *Current Eye Research*, *45*, 339–348. https://doi.org/10.1080/02713683.2019.1648831

Ekstrom, P., Sanyal, S., Narfstrom, K., Chader, G. J., & van Veen, T. (1988). Accumulation of glial fibrillary acidic protein in Müller radial glia during retinal degeneration. *Investigative Ophthalmology & Visual Science*, *29*, 1363–1371.

Fang, K. M., Chang, W. L., Wang, S. M., Su, M. J., & Wu, M. L. (2008). Arachidonic acid induces both Na^+ and $Ca2^+$ entry resulting in apoptosis. *Journal of Neurochemistry*, *104*, 1177–1189.

Fragoso, Y. D., & Brooks, J. B. B. (2015). Leflunomide and teriflunomide: Altering the metabolism of pyrimidines for the treatment of autoimmune diseases. *Expert Review of Clinical Pharmacology*, *8*, 315–320. https://doi.org/10.1586/17512433.2015.1019343

Gao, H., Luodan, A., Huang, X., Chen, X., & Xu, H. (2021). Müller glia-mediated retinal regeneration. *Molecular Neurobiology*, *58*, 2342–2361. https://doi.org/10.1007/s12035-020-02274-w

Gargini, C., Terzibasi, E., Mazzoni, F., & Strettoi, E. (2007). Retinal organization in the retinal degeneration 10 (rd10) mutant mouse: A morphological and ERG study. *The Journal of Comparative Neurology*, *500*, 222–238.

Grant, B. J., Rodrigues, A. P. C., ElSawy, K. M., McCammon, J. A., & Caves, L. S. D. (2006). Bio3d: An R package for the comparative analysis of protein structures. *Bioinformatics*, *22*, 2695–2696.

Green, D. R., & Reed, J. C. (1998). Mitochondria and apoptosis. *Science*, *31*, 118.

Harder, E., Damm W., Maple, J., Wu, C., Reboul, M., Xiang, J., Wang, L., Lupyan, D., Dahlgren, M., Knight, J., Kaus, J., Cerutti, D., Krilov, G., Jorgensen, W., Abel, R., & Friesner, R. (2015). OPLS3: A force field providing broad coverage of drug-like small molecules and proteins. *Journal of Chemical Theory and Computation*, *12*, 281–296. https://doi.org/10.1021/acs.jctc.5b00864

Heise, N., Palme, D., Misovic, M., Koka, S., Rudner, J., Lang, F., Salih, H. R., Huber, S. M., & Henke, G. (2010). Non-selective cation channel-mediated Ca2+−entry and activation of Ca2+/calmodulin-dependent kinase II contribute to G2/M cell cycle arrest and survival of irradiated leukemia cells. *Cellular Physiology and Biochemistry*, *26*, 597–608.

Henke, N., Albrecht, P., Bouchachia, I., Ryazantseva, M., Knoll, K., Lewerenz, J., Kaznacheyeva, E., Maher, P., & Methner, A. (2013). The plasma membrane channel ORAI1 mediates detrimental calcium influx caused by endogenous oxidative stress. *Cell Death & Disease*, *4*, e470.

Herse, P. (2005). Retinitis pigmentosa: Visual function and multidisciplinary management. *Clinical & Experimental Optometry*, *88*, 335–350.

Hood, D. C., Lazow, M. A., Locke, K. G., Greenstein, V. C., & Birch, D. G. (2011). The transition zone between healthy and diseased retina in patients with retinitis pigmentosa. *Investigative Ophthalmology & Visual Science*, *52*, 101–108.

Hoover, W. G. (1985). Canonical dynamics: Equilibrium phase-space distributions. *Physical Review A*, *31*, 1695–1697.

Hou, X., Pedi, L., Diver, M. M., & Long, S. B. (2012). Crystal structure of the calcium release-activated calcium channel Orai. *Science*, *338*, 1308–1313.

Jacobson, M. P., Pincus, D. L., Rapp, C. S., Day, T. J. F., Honig, B., Shaw, D. E., & Friesner, R. A. (2004). A hierarchical approach to all-atom protein loop prediction. *Proteins: Structure, Function, and Bioinformatics*, 55, 351–367.

Jarmula, A., Łusakowska, A., Fichna, J.P., Topolewska, M., Macias, A., Johnson, K., Töpf, A., Straub, V., Rosiak E., Szczepaniak, K., Dunin-Horkawicz, S., Maruszak, A., Kaminska, A., & Redowicz, M. J. (2019). ANO5 mutations in the polish limb girdle muscular dystrophy patients: Effects on the protein structure. *Scientific Reports*, 9, 1–17.

Jo, A. O., Ryskamp, D. A., Phuong, T. T., Verkman, A. S., Yarishkin, O., MacAulay, N., & Križaj, D. (2015). TRPV4 and AQP4 channels synergistically regulate cell volume and calcium homeostasis in retinal Müller glia. *Journal of Neuroscience*, 35, 13525-13537. https://doi.org/10.1523/JNEUROSCI.1987-15.2015

Keirstead, S. A., & Miller, R. F. (1995). Calcium waves in dissociated retinal glial (Müller) cells are evoked by release of calcium from intracellular stores. *Glia*, 14, 14–22.

Khakh, B. S., & McCarthy, K. D. (2015). Astrocyte calcium signaling: From observations to functions and the challenges therein. *Cold Spring Harbor Perspectives in Biology*, 7, a020404.

Klicic Klicic, J. J., Friesner, R. A., Liu, S.-Y., & Guida, W. C. (2002). Accurate prediction of acidity constants in aqueous solution via density functional theory and self-consistent reaction field methods. *The Journal of Physical Chemistry A*, 106, 1327–1335. https://doi.org/10.1021/jp012533f

Lang, F., Friedrich, F., Kahn, E., Wöll, E., Hammerer, M., Waldegger, S., Maly, K., & Grunicke, H. (1991). Bradykinin-induced oscillations of cell membrane potential in cells expressing the Ha-ras oncogene. *Journal of Biological Chemistry*, 266, 4938–4942.

Lang, F., & Hoffmann, E. K. (2012). Role of ion transport in control of apoptotic cell death. *Comprehensive Physiology*, 2, 2037–2061.

Li, J., Abel, R., Zhu, K., Cao, Y., Zhao, S., & Friesner, R. A. (2011). The VSGB 2.0 model: A next generation energy model for high resolution protein structure modeling. *Proteins: Structure, Function and Bioinformatics*, 79, 2794–2812.

Liao, Y., Abramowitz, J., & Birnbaumer, L. (2014). The TRPC family of TRP channels: Roles inferred (mostly) from knockout mice and relationship to ORAI proteins. *Handbook of Experimental Pharmacology*, 223, 1055–1075.

Liou, J., Kim, M. L., do Heo, W., Jones, J. T., Myers, J. W., Ferrell, J. E., Jr., & Meyer, T. (2005). STIM is a Ca2+ sensor essential for Ca2+−store-depletion-triggered Ca2+ influx. *Current Biology*, 15, 1235–1241.

Lomize, M. A., Pogozheva, I. D., Joo, H., Mosberg, H. I., & Lomize, A. L. (2012). OPM database and PPM web server: Resources for positioning of proteins in membranes. *Nucleic Acids Research*, 40, D370–D376.

Madhavi Sastry, G., Adzhigirey, M., Day, T., Annabhimoju, R., & Sherman, W. (2013). Protein and ligand preparation: parameters, protocols, and influence on virtual screening enrichments. *Journal of Computer-Aided Molecular Design*, 27, 221–234. https://doi.org/10.1007/s10822-013-9644-8

Martínez-Fernández de la Cámara, C., Sequedo, M. D., Gómez-Pinedo, U., Jaijo, T., Aller, E., García-Tárraga, P., García-Verdugo, J. M., Millán, J. M., & Rodrigo, R. (2013). Phosphodiesterase inhibition induces retinal degeneration, oxidative stress and inflammation in cone-enriched cultures of porcine retina. *Experimental Eye Research*, 111, 122–133.

Martyna, G. J., Tobias, D. J., & Klein, M. L. (1998). Constant pressure molecular dynamics algorithms. *The Journal of Chemical Physics*, 101, 4177–4189.

Miller, A. (2020). COVID-19: Not just an acute illness. *Trends in Urology & Men's Health*, 11, 17–19.

Molnár, T., Yarishkin, O., Iuso, A., Barabas, P., Jones, B., Marc, R. E., Phuong, T. T., & Križaj, D. (2016). Store-operated calcium entry in Müller glia is controlled by synergistic activation of TRPC and Orai channels. *Journal of Neuroscience*, 36, 3184–3198. https://doi.org/10.1523/JNEUROSCI.4069-15.2016

Nakazawa, M. (2011). Effects of calcium ion, calpains, and calcium channel blockers on retinitis pigmentosa. *Journal of Ophthalmology*, 2011, 1–7.

Newman, E. A. (2015). Glial cell regulation of neuronal activity and blood flow in the retina by release of gliotransmitters. *Philosophical Transactions of the Royal Society of London. Series B, Biological Sciences*, 370, 1–9.

Newman, E. A., & Zahs, K. R. (1998). Modulation of neuronal activity by glial cells in the retina. *Journal of Neuroscience*, 18, 4022–4028.

Olsson, M. H. M., Søndergaard, C. R., Rostkowski, M., & Jensen, J. H. (2011). PROPKA3: Consistent treatment of internal and surface residues in empirical pK a predictions. *Journal of Chemical Theory and Computation*, 7, 525–537. https://doi.org/10.1021/ct100578z

Parekh, A. B. (2017). Regulation of CRAC channels by Ca2+-dependent inactivation. *Cell Calcium*, 63, 20–23.

Parekh, A. B., & Penner, R. (1997). Store depletion and calcium influx. *Physiological Reviews*, 77, 901–930.

Parkash, J., & Asotra, K. (2010). Calcium wave signaling in cancer cells. *Life Sciences*, 87, 587–595.

Phuong, T. T. T., Yarishkin, O., & Križaj, D. (2016). Subcellular propagation of calcium waves in Müller glia does not require autocrine/paracrine purinergic signaling. *Channels*, 10, 421–427. https://doi.org/10.1080/19336950.2016.1193276

Prakriya, M., & Lewis, R. S. (2001). Potentiation and inhibition of Ca2+ release-activated Ca2+ channels by 2-aminoethyldiphenyl borate (2-APB) occurs independently of IP3 receptors. *The Journal of Physiology*, 536, 3–19.

Puro, D. G., Roberget, F., & Chant, C.-C. (1989). Retinal glial cell proliferation and ion channels: A possible link. *Investigative Ophthalmology & Visual Science*, 30, 521–529.

Putney, J. W. (2007). New molecular players in capacitative Ca2+ entry. *Journal of Cell Science*, 120, 1959.

Raman, S., Vernon, R., Thompson, J., Tyka, M., Sadreyev, R., Pei, J., Kim, D., Kellogg, E., DiMaio, F., Lange, O., Kinch, L., Sheffler, W., Kim, B. H., das, R., Grishin, N. V., & Baker, D. (2009). Structure prediction for CASP8 with all-atom refinement using Rosetta. *Proteins*, 77(9), 89–99.

Reichenbach, A., & Bringmann, A. (2013). New functions of Müller cells. *Glia*, 61, 651–678.

Reichenbach, A., & Bringmann, A. (2020). Glia of the human retina. *Glia*, 68, 768–796. https://doi.org/10.1002/glia.23727

Rosado, J. A., Diez, R., Smani, T., & Jardín, I. (2016). STIM and orai1 variants in store-operated calcium entry. *Frontiers in Pharmacology*, 6, 325.

Ryskamp, D. A., Iuso, A., & Križaj, D. (2015). TRPV4 links inflammatory signaling and neuroglial swelling. *Channels*, 9, 70–72. https://doi.org/10.1080/19336950.2015.1017998

Sahaboglu, A., Paquet-Durand, O., Dietter, J., Dengler, K., Bernhard-Kurz, S., Ekström, P. A., Hitzmann, B., Ueffing, M., & Paquet-Durand, F. (2013). Retinitis pigmentosa: Rapid neurodegeneration is governed by slow cell death mechanisms. *Cell Death & Disease*, 4, e488.

Sahaboglu, A., Barth, M., Secer, E., del Amo, E. M., Urtti, A., Arsenijevic, Y., Zrenner, E., & Paquet-Durdand, F. (2016). Olaparib significantly delays photoreceptor loss in a model for hereditary retinal degeneration. *Scientific Reports*, 6, 1–11.

Sakamoto, K., Mccluskey, M., Wensel, T. G., Naggert, J. K., & Nishina, P. M. (2009). New mouse models for recessive retinitis pigmentosa caused by mutations in the Pde6a gene. *Human Molecular Genetics*, 18, 178–192.

Sánchez-Vallejo, V., Benlloch-Navarro, S., Trachsel-Moncho, L., López-Pedrajas, R., Almansa, I., Romero, F. J., & Miranda, M. (2016). Alterations in glutamate cysteine ligase content in the retina of two retinitis pigmentosa animal models. *Free Radical Biology & Medicine*, 96, 245–254.

Shelley, J. C., Cholleti, A., Frye, L. L., Greenwood, J. R., Timlin, M. R., & Uchimaya, M. (2007). Epik: A software program for pKa prediction and

protonation state generation for drug-like molecules. *Journal of Computer-Aided Molecular Design*, 21, 681–691.

Song, Y., DiMaio, F., Wang, R. Y. R., Kim, D., Miles, C., Brunette, T. J., Thompson, J., & Baker, D. (2013). High-resolution comparative modeling with RosettaCM. *Structure*, 21, 1735–1742.

Stauderman, K. A. (2014). CRAC channels as targets for drug discovery and development. *Cell Calcium*, 74, 147–159. https://doi.org/10.1016/j.ceca.2018.07.005

Szikra, T., Barabas, P., Bartoletti, T. M., Huang, W., Akopian, A., Thoreson, W. B., & Krizaj, D. (2009). Calcium homeostasis and cone signaling are regulated by interactions between calcium stores and plasma membrane ion channels. *PLoS One*, 4, e6723.

Szikra, T., Cusato, K., Thoreson, W. B., Barabas, P., Bartoletti, T. M., & Krizaj, D. (2008). Depletion of calcium stores regulates calcium influx and signal transmission in rod photoreceptors. *The Journal of Physiology*, 586, 4859–4875.

Tanito, M., Elliott, M. H., Kotake, Y., & Anderson, R. E. (2005). Protein modifications by 4-hydroxynonenal and 4-hydroxyhexenal in light-exposed rat. *Retina*, 46, 3859–3868.

Taylor, J. T., Zeng, X. B., Pottle, J. E., Lee, K., Wang, A. R., Yi, S. G., Scruggs, J. A. S., Sikka, S. S., & Li, M. (2008). Calcium signaling and T-type calcium channels in cancer cell cycling. *World Journal of Gastroenterology*, 14, 4984–4991.

Toft-Kehler, A. K., Gurubaran, I. S., Desler, C., Rasmussen, L. J., Skytt, D. M., & Kolko, M. (2016). Oxidative stress-induced dysfunction of Müller cells during starvation. *Investigative Ophthalmology & Visual Science*, 57, 2721–2728.

Trachsel-Moncho, L., Benlloch-Navarro, S., Fernández-Carbonell, A., Ramírez-Lamelas, A. T., Olivar, T., Silvestre, D., Poch, E., & Miranda M. (2018). Oxidative stress and autophagy-related changes during retinal degeneration and development. *Cell Death & Disease*, 9, 1–12.

Tsang, S. H., & Sharma, T. (2018). Retinitis pigmentosa (non-syndromic). *Advances in Experimental Medicine and Biology*, 1085, 125–130.

Tuckerman, M., Berne, B. J., & Martyna, G. J. (1992). Reversible multiple time scale molecular dynamics. *The Journal of Chemical Physics*, 97, 1990–2001.

Uhlén, M., Fagerberg, L., Hallström, B. M., Lindskog, C., Oksvold, P., Mardinoglu, A., Sivertsson, A., Kampf, C., Sjöstedt, E., Asplund, A., Olsson, I. M., Edlund, K., Lundberg, E., Navani, S., Szigyarto, C. A. K., Odeberg, J., Djureinovic, D., Takanen, J.O., Hober, S., ... Pontén, F. (2015). Tissue-based map of the human proteome. *Science*, 347, 1260419.

Vaca, L. (2010). SOCIC: The store-operated calcium influx complex. *Cell Calcium*, 47, 199–209.

Verkhratsky, A., et al. (2013). TRP channels coordinate ion signalling in astroglia. *Reviews of Physiology, Biochemistry and Pharmacology*, 166, 1–22. https://doi.org/10.1007/112_2013_15

Vidal-Gil, L., Sancho-Pelluz, J., Zrenner, E., Oltra, M., & Sahaboglu, A. (2019). Poly ADP ribosylation and extracellular vesicle activity in rod photoreceptor degeneration. *Scientific Reports*, 9, 1–10.

Wang, T., Reingruber, J., Woodruff, M. L., Majumder, A., Camarena, A., Artemyev, N. O., Fain, G. L., & Chen, J. (2018). The PDE6 mutation in the rd10 retinal degeneration mouse model causes protein mislocalization and instability and promotes cell death through increased ion influx. *The Journal of Biological Chemistry*, 293, 15332–15346.

Wert, K. J., Lin, J. H., Tsang, S. H., Brown Glaucoma Laboratory, & Harkness, E. S. (2014). General pathophysiology in retinal degeneration HHS public access. *Developments in Ophthalmology*, 53, 33–43.

Yamashita, M., Yeung, P. S.-W., Ing, C. E., McNally, B. A., Pomes, R., & Prakriya, M. (2017). STIM1 activates CRAC channels through rotation of the pore helix to open a hydrophobic gate. *Nature Communications*, 8, 1–13.

Yan, J., Hosseinzadeh, Z., Zhang, B., Froeschl, M., Schulze-Osthoff, K., Stournaras, C., & Lang, F. (2016). Decrease of Store-Operated Ca^{2+} Entry and Increase of Na^+/Ca^{2+} Exchange by Pharmacological JAK2 Inhibition. *Cell Physiol Biochem*. 38(2), 683–695. https://doi.org/10.1159/000443126

Yan, J., Zhang, B., Hosseinzadeh, Z., & Lang, F. (2016). Down-Regulation of Store-Operated Ca^{2+} Entry and $Na^+ Ca^{2+}$ Exchange in MCF-7 Breast Cancer Cells by Pharmacological JAK3 Inhibition. *Cell Physiol Biochem*, 38, 1643–51.

Yelshanskaya, M., Nadezhdin, K. D., Kurnikova, M. G. & Sobolevsky, A. I. (2021). Structure and function of the calcium-selective TRP channel TRPV6. *The Journal of Physiology* 599, 2673–2697.

Yeung, P. S. W., Ing, C. E., Yamashita, M., Pomès, R., & Prakriya, M. (2020). A sulfur-aromatic gate latch is essential for opening of the orai1 channel pore. *eLife*, 9, 1–18.

Zhang, X., Feng, Q., & Cote, R. H. (2005). Efficacy and selectivity of phosphodiesterase-targeted drugs in inhibiting photoreceptor phosphodiesterase (PDE6). *Retinal Photoreceptors*, 46, 3060–3066. https://doi.org/10.1167/iovs.05-0257

Zhong, Q., Mishra, M., & Kowluru, R. A. (2013). Transcription factor Nrf2-mediated antioxidant defense system in the development of diabetic retinopathy. *Investigative Ophthalmology & Visual Science*, 54, 3941–3948.

SUPPORTING INFORMATION

Additional supporting information can be found online in the Supporting Information section at the end of this article.